A Prospective Comparison of ^{18}F-Sodium Fluoride PET/CT and PSMA-Targeted ^{18}F-DCFBC PET/CT in Metastatic Prostate Cancer

Stephanie A. Harmon[1], Ethan Bergvall[2], Esther Mena[2], Joanna H. Shih[3], Stephen Adler[1], Yolanda McKinney[2], Sherif Mehralivand[2], Deborah E. Citrin[4], Anna Couvillon[5], Ravi A. Madan[5], James L. Gulley[5], Ronnie C. Mease[6], Paula M. Jacobs[7], Martin G. Pomper[6], Baris Turkbey[2], Peter L. Choyke[2], and M. Liza Lindenberg[2]

[1]Clinical Research Directorate/Clinical Monitoring Research Program, Leidos Biomedical Research, Inc., National Cancer Institute, Campus at Frederick, Frederick, Maryland; [2]Molecular Imaging Program, National Cancer Institute, National Institutes of Health, Bethesda, Maryland; [3]Division of Cancer Treatment and Diagnosis: Biometric Research Program, National Cancer Institute, National Institutes of Health, Bethesda, Maryland; [4]Radiation Oncology Branch, National Cancer Institute, National Institutes of Health, Bethesda, Maryland; [5]Genitourinary Malignancies Branch, National Cancer Institute, National Institutes of Health, Bethesda, Maryland; [6]Russell H. Morgan Department of Radiology and Radiological Science, Johns Hopkins University School of Medicine, Baltimore, Maryland; and [7]Cancer Imaging Program, National Cancer Institute, National Institutes of Health, Rockville, Maryland

The purpose of this study was to compare the diagnostic performance of ^{18}F-DCFBC PET/CT, a first-generation ^{18}F-labeled prostate-specific membrane antigen (PSMA)–targeted agent, and ^{18}F-NaF PET/CT, a sensitive marker of osteoblastic activity, in a prospective cohort of patients with metastatic prostate cancer. **Methods:** Twenty-eight prostate cancer patients with metastatic disease on conventional imaging prospectively received up to 4 PET/CT scans. All patients completed baseline ^{18}F-DCFBC PET/CT and ^{18}F-NaF PET/CT scans, and 23 patients completed follow-up imaging, with a median follow-up interval of 5.7 mo (range, 4.2–12.6 mo). Lesion detection was compared across the 2 PET/CT agents at each time point. Detection and SUV characteristics of each PET/CT agent were compared with serum prostate-specific antigen (PSA) levels and treatment status at the time of baseline imaging using nonparametric statistical testing (Spearman correlation, Wilcoxon rank). **Results:** Twenty-six patients had metastatic disease detected on ^{18}F-NaF or ^{18}F-DCFBC at baseline, and 2 patients were negative on both scans. Three patients demonstrated soft tissue–only disease. Of 241 lesions detected at baseline, 56 were soft-tissue lesions identified by ^{18}F-DCFBC only and 185 bone lesions detected on ^{18}F-NaF or ^{18}F-DCFBC. ^{18}F-NaF detected significantly more bone lesions than ^{18}F-DCFBC ($P < 0.001$). Correlation of PSA with patient-level SUV metrics was strong in ^{18}F-DCFBC ($\rho > 0.5$, $P < 0.01$) and poor in ^{18}F-NaF ($\rho < 0.3$, $P > 0.1$). When PSA levels were combined with treatment status, patients with below-median levels of PSA (<2 ng/mL) on androgen deprivation therapy ($n = 11$) demonstrated more lesions on ^{18}F-NaF than ^{18}F-DCFBC ($P = 0.02$). In PSA greater than 2 ng/mL, patients on androgen deprivation therapy ($n = 8$) showed equal to or more lesions on ^{18}F-DCFBC than on ^{18}F-NaF. **Conclusion:** The utility of PSMA-targeting imaging in metastatic prostate cancer appears to depend on patient disease course and treatment status. Compared with ^{18}F-NaF PET/CT, ^{18}F-DCFBC PET/CT detected significantly fewer bone lesions in the setting of early or metastatic castrate-sensitive disease on treatment. However, in advanced metastatic castrate-resistant prostate cancer, ^{18}F-DCFBC PET/CT shows good concordance with NaF PET/CT.

Key Words: PSMA; NaF; metastatic prostate cancer; PET/CT imaging

J Nucl Med 2018; 59:1665–1671
DOI: 10.2967/jnumed.117.207373

Despite the promising decline in overall prostate cancer mortality rates in recent decades, disease-specific survival has not improved in men with metastatic prostate cancer (*1*). Clinical trial design is limited by the lack of predictive biomarkers, including imaging-based biomarkers, in this setting. Conventional imaging modalities such as CT, MRI, and ^{99m}Tc-methylene diphosphonate bone scintigraphy (bone scan) have shown modest, yet incomplete, prediction of treatment success (*2,3*).

Several molecular targets have shown promise in assessing disease burden. ^{18}F-labeled sodium fluoride (^{18}F-NaF) is a highly sensitive PET agent targeting bone turnover for detection of skeletal metastases (*4,5*). ^{18}F-NaF PET/CT has a sensitivity superior to conventional planar bone scans, although its specificity is limited by false-positive benign bone pathologies (*6*). Gaining recent attention are newer radioligands targeting prostate-specific membrane antigen (PSMA), a transmembrane protein highly expressed in prostate cancer cells, which is thought to correlate with disease aggressiveness (*7,8*). PSMA-targeting PET agents have shown promising clinical utility in biochemically recurrent disease (*9–11*). Initial studies in metastatic prostate cancer show superior sensitivity compared with conventional imaging modalities and there is great hope that PSMA-targeted imaging can serve as an accurate imaging biomarker of disease burden in metastatic prostate cancer (*12–14*).

There are limited data on the comparative performance of PSMA-targeted imaging with ^{18}F-NaF PET/CT, though initial case reports in advanced metastatic castrate-resistance (CRPC) suggest a diagnostic advantage of PSMA-targeted PET/CT (*15,16*). Here, we

Received Dec. 21, 2017; revision accepted Mar. 21, 2018.
For correspondence or reprints contact: Stephanie Harmon, National Institutes of Health, Building 10, Room B3B85, Bethesda, MD 20892.
E-mail: stephanie.harmon@nih.gov
Published online Mar. 30, 2018.

present a prospective pilot study comparing the detection performance of PSMA-targeted PET/CT using ^{18}F-DCFBC, a first-generation ^{18}F-labeled small molecule targeting the external binding domain of PSMA (*12,17*), with ^{18}F-NaF PET/CT in metastatic prostate cancer patients.

MATERIALS AND METHODS

Patient Population

This single-institution prospective study was approved by the Institutional Review Board and was Health Insurance Portability and Accountability Act–compliant (NCT02190279). All patients enrolled after written informed consent was obtained. The primary objective of the multiarm study was to assess ^{18}F-DCFBC in localized, recurrent and metastatic prostate cancer. We report findings from the metastatic population, with secondary endpoint to compare uptake of ^{18}F-DCFBC in bone with ^{18}F-NaF PET/CT. Eligibility required histopathologically confirmed prostate cancer and identifiable metastatic disease on conventional imaging (CT, MRI, or bone scan). All patients underwent baseline ^{18}F-DCFBC PET/CT and ^{18}F-NaF PET/CT scans (median interval, 7 d). Follow-up scans were obtained at a median 5.7 mo (range, 4.2–12.6 mo) after baseline imaging. There was no exclusion criteria regarding prior or ongoing therapies. Castration status, all prior treatment history, diagnostic history, and current treatments were established on the basis of clinical review of patient medical records. Prostate-specific antigen (PSA) levels were obtained at baseline and at the time of follow-up imaging. Interval treatments occurring between baseline and follow-up imaging time points were documented. Change in PSA during treatment was evaluated by PSA fold change, defined as the ratio of follow-up PSA to baseline PSA.

PET/CT Acquisition

^{18}F-DCFBC was produced on a FASTlab synthesizer according to good-manufacturing-practice procedures, as described previously (*17,18*). Patients received ^{18}F-DCFBC administered as an intravenous bolus (range, 277–296 MBq) followed by static whole-body PET/CT performed at 60 min (range, 52–66 min) and 120 min (range, 107–141 min) after injection. ^{18}F-NaF was commercially obtained (Cardinal Health). A single, static whole-body ^{18}F-NaF PET/CT scan was obtained 60 min (range, 50–81 min) after intravenous bolus of radiotracer (range, 99–137 MBq). All imaging was performed on a Gemini TF system (Philips Healthcare). Low-dose CT transmission scans were obtained (120 kVp, 60 mAs, 0.75-s rotation time, 1.438 pitch, axial slice thickness of 5 mm) for attenuation correction and localization. Emission PET images were obtained at 2 min/bed position with 22 slices in bed overlap. The PET images were reconstructed using the Gemini TF's (*19*) default reconstruction algorithm (BLOB-OS-TF, a 3-dimensional ordered subset iterative time-of-flight reconstruction technique using 3 iterations, 33 subsets, and a voxel size of $4 \times 4 \times 4$ mm). SUVs were calculated as the ratio of measured activity to injected dose per kilogram of patient's body weight.

PET/CT Analysis

Imaging review and analysis was performed using commercial software (MIM). Three nuclear medicine physicians independently reviewed ^{18}F-DCFBC PET/CT and ^{18}F-NaF PET/CT images for identification of regions suggestive of metastatic disease. Only lesions that were determined to be highly suggestive of metastatic disease by reader consensus were included in this study. This process was repeated for follow-up imaging. SUV_{max} was reported for each lesion identified. Within each patient, the SUV_{max} and SUV_{mean} uptake were calculated from all reported lesions. The total uptake burden, SUV_{total}, was calculated as the sum of lesion-SUV_{total} ($SUV_{mean} \times$ volume) derived from threshold containing 80% of SUV_{max} from all reported lesions. Response was calculated as the percentage change from baseline to follow-up imaging.

TABLE 1
Study Demographics

Characteristic	Data
Median age (y)	65 (range, 42–91)
Gleason grade at initial diagnosis (*n*)	
6	7 (25%)
7–8	11 (39%)
9–10	9 (32%)
Not available	1 (4%)
Prior prostate cancer therapy (*n*)	
None	4 (14%)
Radical prostatectomy	12 (43%)
Brachytherapy	1 (4%)
Radiation	11 (39%)
ADT	19 (68%)
Chemotherapy	6 (21%)
^{223}Ra	1 (4%)
Castration status (*n*)	
Untreated	3 (11%)
Castrate-sensitive	14 (50%)
Castrate-resistant	11 (39%)
Median PSA at baseline (ng/mL)	2.08 (range, 0.07–4,379)
Therapy at baseline (*n*)	
No treatment	9 (32%)
ADT	16 (57%)
ADT + other	3 (11%)
Median PSA at follow-up (ng/mL)	0.76 (0.02–1,046)
Therapy in scan interval (*n*)	
No treatment	3 (13%)
ADT	14 (61%)
ADT + other	6 (26%)
Baseline imaging (*n*)	
NaF PET/CT	28 (100%)
DCFBC (1 h) PET/CT	28 (100%)
DCFBC (2 h) PET/CT	27 (96%)
Follow-up imaging (*n*)	
NaF PET/CT	23 (100%)
DCFBC (1 h) PET/CT	22 (96%)
DCFBC (2 h) PET/CT	23 (100%)

Statistical Analysis

^{18}F-DCFBC and ^{18}F-NaF characteristics (number of lesions, SUV statistics) were correlated to PSA values using Spearman rank correlation. Differences in imaging characteristics across patient status characteristics, such as treatment status and castration status, were evaluated using the Wilcoxon rank-sum or signed-rank tests, when appropriate. The number of detected bone lesions by ^{18}F-NaF PET/CT and ^{18}F-DCFBC PET/CT was compared by the sign test. Correlation of lesion-level statistics across tracers was performed by Spearman correlation estimation for

TABLE 2
DCFBC Bone Lesion Detection for 1- and 2-Hour Time Points at Baseline and Follow-up Imaging

Scan time point	^{18}F-DCFBC time point (no. of patients)	Bone lesion detection			
		^{18}F-DCFBC only	Concordant	^{18}F-NaF only	Proportion detected
Baseline	DCFBC (1 h) (n = 28)	3	81	101	45.4%
	DCFBC (2 h) (n = 27)	3	82	96	45.9%
Follow-up	DCFBC (1 h) (n = 22)	25	51	65	51.7%
	DCFBC (2 h) (n = 23)	25	54	68	53.7%

Bone lesion detection characterized as DCFBC only, concordant (DCFBC and NaF), and NaF only. Proportion detected calculated as ratio of DCFBC detected bone lesions to all detected bone lesions.

clustered data (*20*). Lesions were categorized as concordant or discordant across tracers, and uptake characteristics were compared using Wilcoxon rank-sum test for clustered data (*21*). All tests were 2-sided, and P values of less than 0.05 were considered statistically significant.

RESULTS

Patient demographics are listed in Table 1. At baseline, 9 patients were not on treatment, 16 were on androgen deprivation therapy (ADT) and 3 patients were on ADT + chemotherapy. In total, 26 of 28 patients had metastatic disease detected on ^{18}F-NaF (n = 22) or ^{18}F-DCFBC (n = 15) at baseline, and 21 of 23 had findings on ^{18}F-NaF (n = 19) or ^{18}F-DCFBC (n = 13) at follow-up. As determined by imaging in this study, 3 patients had soft tissue–only metastases, 14 had bone-only disease, and 9 had both soft-tissue and bone disease. The study summary is provided in Supplemental Table 1 (supplemental materials are available at http://jnm.snmjournals.org).

Lesion Detection

In total, 241 lesions were detected, with 56 soft-tissue lesions identified by ^{18}F-DCFBC only and 185 bone lesions detected on ^{18}F-NaF or ^{18}F-DCFBC. Table 2 summarizes bone lesion detection by tracer at each time point. At baseline, ^{18}F-NaF detected 182 of 185 (98.4%) of bone lesions, significantly higher than ^{18}F-DCFBC at 1 h (45.4%, $P < 0.001$) and ^{18}F-DCFBC at 2 h (45.9%, $P < 0.001$). These differences were maintained at follow-up imaging. ^{18}F-DCFBC identified 3 bone lesions that did not have focal uptake on ^{18}F-NaF at baseline and 25 lesions that were not seen on ^{18}F-NaF images at follow-up, all within a single patient with advanced CRPC (Fig. 1). No differences in lesion detection were noted across ^{18}F-DCFBC after injection time points so the 2-h time point was considered only for the remainder of the analysis.

Bone Lesion Uptake

Lesion-level ^{18}F-NaF SUV_{max} and ^{18}F-DCFBC (2 h) SUV_{max} were not significantly correlated at baseline ($\rho = 0.41$, $P = 0.095$) or follow-up ($\rho = 0.29$, $P = 0.29$) (Fig. 2). Lesion-level ^{18}F-NaF SUV_{max} was lower in bone lesions detected only by ^{18}F-NaF than ^{18}F-NaF SUV_{max} in bone lesions detected by both tracers, nearing significance at baseline ($P = 0.06$) and significant at follow-up ($P = 0.006$) (Table 3). This trend was not noted for ^{18}F-DCFBC (2 h) SUV_{max} characteristics.

Correlation to PSA

Median PSA was 2.08 ng/mL (range, 0.01–4379 ng/mL) at baseline imaging and 0.76 ng/mL (range, 0.015–1046 ng/mL) at follow-up. At baseline imaging, patient-level ^{18}F-DCFBC (2 h) uptake characteristics showed significant correlation with PSA levels, with the strongest correlation with the number of lesions ($\rho = 0.60$, $P = 0.001$) and SUV_{total} ($\rho = 0.58$, $P = 0.003$), whereas patient-level ^{18}F-NaF uptake characteristics showed weak correlation to baseline PSA (Table 4; Supplemental Fig. 1). This was maintained at the follow-up imaging time point. For patients receiving treatment in the interim between baseline and follow-up imaging (n = 18), 5 experienced increasing PSA (fold change > 1).

Correlation to Disease Status

In general, an increasing number of lesions were detected by both tracers as the disease became more advanced, ranging from patients with no treatment at baseline to those with advanced second-line combinations of ADT + chemotherapy (Fig. 3). ^{18}F-NaF detected a higher number of lesions in the group of castrate-sensitive

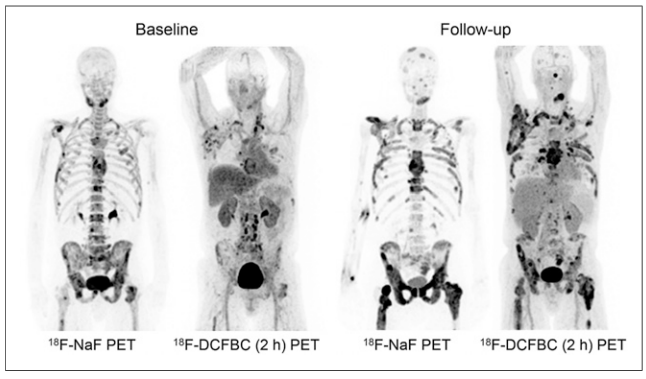

FIGURE 1. A 64-y-old patient diagnosed with de novo metastatic prostate cancer 4 y before enrollment. Prior treatment history included first- and second-line ADT and chemotherapy. Patient was considered to have CRPC with serum PSA of 812.3 ng/mL at time of baseline imaging. ^{18}F-NaF imaging detected 28 bone lesions, with 17 sites concordant with ^{18}F-DCFBC (2 h) imaging. Three bone and 13 soft-tissue sites were positive only on ^{18}F-DCFBC (2 h) imaging. Treatment at time of baseline imaging included ADT + docetaxel that continued until follow-up imaging 7 mo later, at which time PSA had increased to 1,025 ng/mL. At follow-up, both scans showed disease progression. Number of lesions identified only by ^{18}F-DCFBC (2 h) imaging at follow-up included 25 bone and 11 soft-tissue sites.

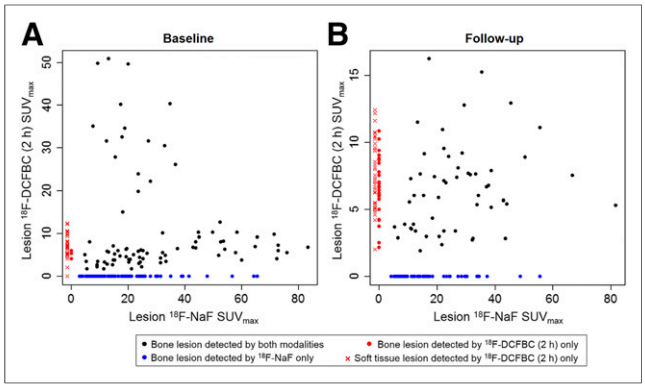

FIGURE 2. Lesion-based correlation of ^{18}F-NaF and ^{18}F-DCFBC SUV_{max} at baseline (A: ρ = 0.41, P = 0.095) and follow-up (B: ρ = 0.29, P = 0.29). Lesions detected only by ^{18}F-NaF PET/CT imaging are shown in blue (assigned ^{18}F-DCFBC [2 h] SUV_{max} = 0), and lesions detected only by ^{18}F-DCFBC (2 h) PET/CT imaging are shown in red (assigned ^{18}F-NaF SUV_{max} = 0), designated by lesion location as soft-tissue (x) or bone (red circle).

+ untreated patients than ^{18}F-DCFBC (2 h) at baseline, nearing statistical significance for all lesions (P = 0.06) and significant for bone-only lesions (P = 0.002) (Figs. 3C and 3D). Patients were then stratified by median PSA value and ADT status, assuming that higher PSA on ADT implied more advanced disease (Fig. 4). The primary difference in detection of metastatic lesions between ^{18}F-NaF and ^{18}F-DCFBC (2 h) at baseline was found to occur in patients with a PSA of less than 2 ng/mL who were on ADT at the time of imaging, where ^{18}F-NaF was able to detect significantly more sites of disease in such patients (P = 0.02 for all lesions and 0.01 for bone lesions in Figs. 4A and 4B, respectively). The most extreme example in this group is highlighted in Figure 5. As PSA advanced beyond 2.0 ng/mL, the number of lesions detected using ^{18}F-DCFBC PET/CT equaled or exceeded the number of lesions found with ^{18}F-NaF PET/CT (Fig. 1; Supplemental Fig. 2).

Pathologic Validation

Pathology results were obtained for 6 patients (7 lesions) within 2 mo of study imaging. Of 4 bone lesions, ^{18}F-NaF demonstrated 2 false-positives (both iliac lesions) and 2 true-positives (rib, sacrum) whereas ^{18}F-DCFBC had 1 false-positive (iliac), 1 true-negative (iliac), and 2 false-negatives (rib, sacrum). Of 3 soft-tissue lesions, ^{18}F-DCFBC demonstrated 2 false-negatives (retroperitoneal lymph node, omental lesion) and 1 true-positive (lung).

DISCUSSION

Although PSMA-targeting imaging agents have shown promising sensitivity for recurrent disease after primary cancer treatment, the results in metastatic prostate cancer have yet to be fully characterized. The primary objective of this study was to prospectively explore the detection performance of PSMA-targeted ^{18}F-DCFBC PET/CT in comparison to ^{18}F-NaF PET/CT, a highly sensitive bone scan agent. Within this pilot study, we reported that patient disease and treatment status may influence the diagnostic ability of ^{18}F-DCFBC PET/CT in patients with metastatic disease.

Overall, ^{18}F-NaF PET/CT showed higher detection rates than PSMA-targeted ^{18}F-DCFBC PET/CT at baseline, detecting 98.4% versus 45.9% (2-h after injection) of bone lesions, respectively. The lack of centrally reviewed conventional imaging in this study limits direct comparison to previous works in which ^{18}F-DCFBC PET/CT sensitivity was 88%–92% compared with 71%–82% in conventional bone scan, and ^{68}Ga-PSMA PET/CT achieved a 98%–100% sensitivity compared with 82%–86% in conventional bone scan (*12,13*). Similar improvements in sensitivity have been shown for ^{18}F-NaF PET/CT compared with planar bone scans, though specificity is still limited by its indirect surrogacy of prostate cancer in the bone (*6*).

Within this mixed metastatic population, 13 patients had negative ^{18}F-DCFBC scans. The highest discrepancy in modalities was observed in patients early after diagnosis and early after ADT therapy, particularly in hormone-sensitive or minimally symptomatic castrate-resistant disease states (*22*). Literature tends to support the concept that patients on ADT are more likely to have positive findings on PSMA-targeted imaging (*9–11*). However, as noted by others, this finding is likely confounded by patients with advanced castrate-resistant disease who are also still on ADT. We have hypothesized the role of ADT and disease status on imaging findings within Figure 6 and the following discussion.

After beginning first-line ADT, androgen-sensitive cells will demonstrate a decrease in cellular proliferation, resulting in apoptosis in some, but not all, cancer cells (*23,24*). However, prostate cancer bone metastases have often initiated an osteoblastic reaction that persists even after successful ADT (*25,26*). Within this window, it is possible that ADT has suppressed oncogenic activity in PSMA-expressing cells such that imaging is unable to detect remaining senescent cells, whereas ^{18}F-NaF still recognizes bone response. Additionally, bone scan of any type is susceptible to flare in which the osteoblastic reaction briefly increases after

TABLE 3
^{18}F-NaF and ^{18}F-DCFBC (2 Hour) Lesion SUV_{max} at Baseline and Follow-up Imaging in Bone Lesions

Scan time point	Tracer	Bone lesion detection concordance			P
		^{18}F-DCFBC only	Concordant	^{18}F-NaF only	
Baseline	^{18}F-NaF SUV_{max}	–	23.9 (4.72–83.4)	12.3 (2.82–65.3)	0.064
	^{18}F-DCFBC(2 h) SUV_{max}	5.46 (4.17–6.09)	6.01 (1.69–50.85)	–	0.48
Follow-up	NaF SUV_{max}	–	22.7 (5.27–81.8)	13.2 (4.1–55.5)	0.006
	^{18}F-DCFBC(2 h) SUV_{max}	6.59 (2.19–10.84)	6.33 (1.95–16.2)	–	0.64

Data are median, with range in parentheses. Lesions stratified by detection on both modalities: DCFBC only, concordant (DCFBC and NaF), and NaF only. Difference in SUV_{max} across groups assessed using Wilcoxon rank-sum test for clustered data.

TABLE 4
Correlation of PSA with Patient-Level SUV Metrics Derived from ^{18}F-DCFBC (2 Hour) and NaF Uptake at Baseline and Follow-up Imaging, Assessed Using Spearman Correlation Coefficient

	Baseline				Follow-up			
	^{18}F-DCFBC (2 h)		^{18}F-NaF		^{18}F-DCFBC (2 h)		^{18}F-NaF	
Metric	ρ	*P*	ρ	*P*	ρ	*P*	ρ	*P*
$N_{lesions}$	0.60	0.001	0.23	0.26	0.55	0.01	0.063	0.79
SUV_{max}	0.52	0.007	0.27	0.18	0.53	0.013	−0.07	0.77
SUV_{mean}	0.47	0.018	0.28	0.17	0.55	0.0097	−0.18	0.43
SUV_{total}	0.58	0.003	0.21	0.30	0.51	0.017	−0.05	0.83

$N_{lesions}$ = number of detected lesions.

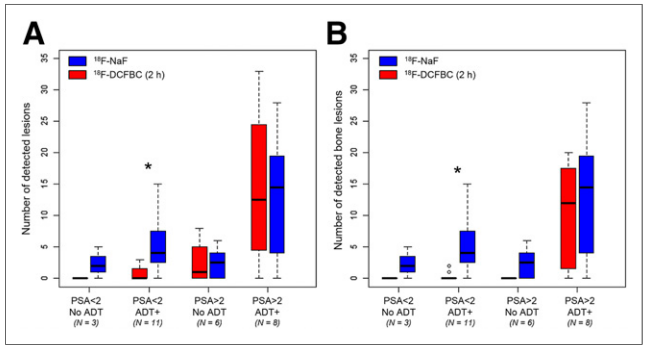

FIGURE 4. Baseline lesion detection stratified by median serum PSA (2 ng/mL) and ADT status (+/−). Patients with low PSA levels not receiving treatment had lowest number of detected lesions for both tracers. In patients receiving treatment and maintaining PSA levels of less than 2 ng/mL, ^{18}F-NaF detected significantly more lesions ^{18}F-DCFBC (2 h) imaging (P = 0.02). In later stages of disease, either by high PSA value (>2 ng/mL) or high PSA and on active treatment, imaging modalities gave similar detection distributions.

initiation of ADT. In this sense, PSMA-targeted PET provides a more accurate assessment of prostate cancer activity, both in bone and soft tissue, reflected in the strong correlation of ^{18}F-DCFBC and PSA in this study. In the absence of treatment, these findings could also support the hypothesis that a small population of prostate cancer cells may amplify the osteoblastic activity so that ^{18}F-NaF detection is possible but still fails to reach the detection threshold of PSMA-targeting agents (*12*).

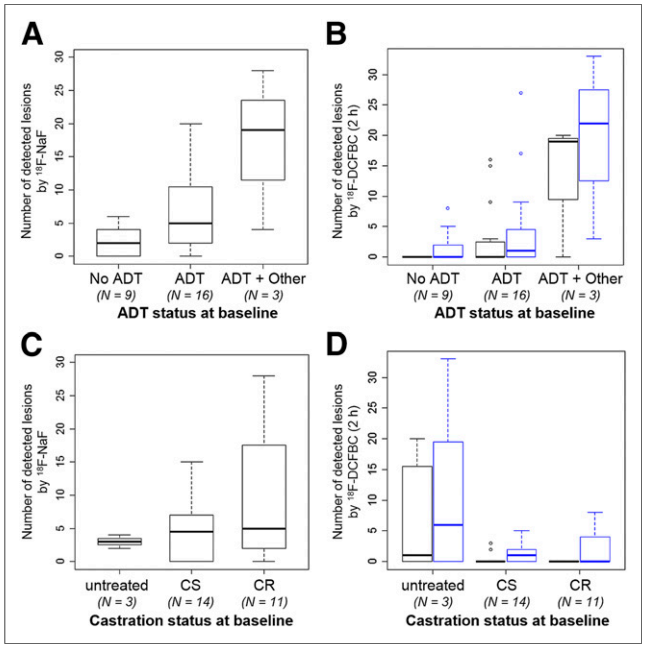

FIGURE 3. Lesion detection stratified by treatment and castration status at baseline imaging for bone lesions (black) and all lesions (blue). ^{18}F-NaF detection at baseline showed strong dependence on ADT status (A) and castration status (C), where worsening disease status (CR or advanced treatments) show higher disease burden. ^{18}F-DCFBC (2 h) detection also showed dependence on ADT status (B) and castration status (D), though similar levels of detection were only noted in most advanced stages of disease. CR = castrate resistant; CS = castrate sensitive.

In later stages of disease, lesion detection was not significantly different across the 2 tracers, particularly in advanced, symptomatic metastatic CRPC disease states (*22*). At the follow-up time point, ^{18}F-DCFBC PET/CT was able to detect more bone lesions than ^{18}F-NaF PET/CT in 1 patient with severe disease progression (Fig. 1). This is in agreement with reports from other PSMA-targeting agents in advanced metastatic CRPC (*13,15,16*). These findings support the literature indicating PSMA expression increases throughout advanced stages of disease (*27*). The metastatic foci positive only on ^{18}F-DCFBC appeared as ground-glass findings on CT, likely demonstrating active tumor invasion with insufficient osteoblastic activity to trigger ^{18}F-NaF uptake. Overall, the findings of this study are important to validate in the future for selection and monitoring of targeted radionuclide therapies, where false-negatives on either PSMA-targeting agents or ^{18}F-NaF imaging could hinder treatment effectiveness.

PSA correlation with number of lesions and SUV characteristics were stronger with ^{18}F-DCFBC imaging than with ^{18}F-NaF imaging at baseline. ^{18}F-NaF is inherently limited to only detecting bone disease, compared with PSMA-targeting agents that can capture the burden of both bone and soft-tissue disease. No treatment regimen was defined by this imaging protocol; therefore, the timing of both treatment and follow-up scans was variable but future studies are needed to explore treatment response assessment with both agents.

FIGURE 5. A 48-y-old patient recently diagnosed with de novo metastatic prostate cancer (serum PSA, 20.11 ng/mL), with pathologic validation of metastases in right sacrum and retroperitoneal lymph nodes. Patient started ADT (degarelix) 1 mo before baseline imaging, at which time his PSA was 1.61 ng/mL. ^{18}F-DCFBC (2 h) PET/CT was negative. ^{18}F-NaF PET/CT showed 15 sites detected as highly likely for harboring metastatic disease (red arrows), as well as other regions of uptake secondary to degenerative or benign processes (not included in analysis).

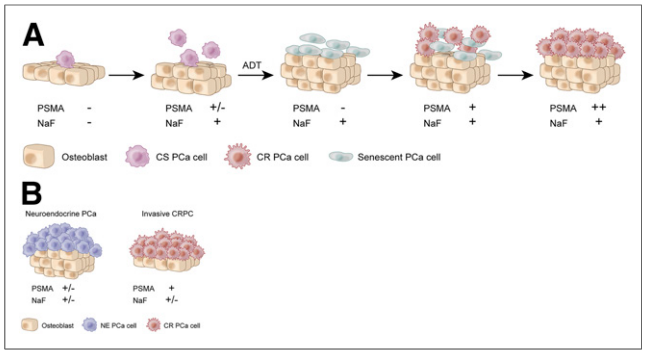

FIGURE 6. (A) Possible association of prostate cancer disease states with imaging characteristics. In early castrate-sensitive disease states, bone metastases are undetectable by both imaging modalities before eliciting an osteoblastic response enabling ^{18}F-NaF detection that may or may not reach detection limits of PSMA depending on number and PSMA expression of prostate cancer cells . After initiation of ADT, lack of PSMA findings could reflect responsive castrate-sensitive disease-causing involution or initial senescence of cancer cells, whereas persistent ^{18}F-NaF findings may detect regions of residual boney reaction. PSMA and ^{18}F-NaF are expected to show concurrent findings as disease advances to castrate-resistant states before progressive growth of advanced castrate-resistant disease after first- and second-line therapies, where PSMA findings may exceed that of ^{18}F-NaF. (B) Other disease states not captured could include neuroendocrine variants of prostate cancer that may be poorly captured by either modality and invasive castrate-resistant disease characterized by extensive bone marrow replacement in end-stage metastatic CRPC with a weakened bone-reaction (30).

There are several limitations within this relatively small study of a heterogeneous population of metastatic prostate cancer patients. Very few histopathologic validation specimens were available for review, as is common in the metastatic setting. Two of 4 bone biopsies were shown to be false-positives on ^{18}F-NaF, reflecting its modest specificity. Additionally, results from biopsy indicated some frequency of false-negative PSMA scans. Importantly, ^{18}F-DCFBC is considered a first-generation PSMA-targeting agent with relatively low binding affinity to PSMA and increased vascular background activity. This may compromise its sensitivity in early disease. A second-generation PSMA-targeting agent, ^{18}F-DCFPyL, possessing higher binding affinity to PSMA and rapid blood clearance, is currently in clinical trials (*14,15,28*). Multiple PSMA-based tracers are currently under development for clinical use in prostate cancer, including ^{99m}Tc, ^{68}Ga, and ^{18}F ligands (*29*). Although the role of PSMA-targeted imaging in the setting of biochemically recurrent disease has been well explored, its role in metastatic disease requires further investigation.

CONCLUSION

In this study, ^{18}F-NaF PET/CT and PSMA-targeting ^{18}F-DCFBC PET/CT were prospectively compared for detection of metastatic disease. Although attractive due to its ability to identify both bone and soft-tissue disease, we present evidence that the utility of PSMA-targeting PET/CT imaging in metastatic prostate cancer appears to depend on patient disease course and treatment status. Notably, ^{18}F-NaF PET/CT and ^{18}F-DCFBC PET/CT were largely concordant in metastatic CRPC. Further research is warranted to elucidate the dependence of disease status and timing of treatment on detection characteristics of PSMA-targeting PET/CT agents.

DISCLOSURE

This project has been funded in whole or in part with federal funds from the National Cancer Institute, National Institutes of Health, under Contract No. HHSN261200800001E. The content of this publication does not necessarily reflect the views or policies of the Department of Health and Human Services, nor does mention of trade names, commercial products, or organizations imply endorsement by the U.S. Government. This project was supported in part by the Intramural Research Program of the NIH and NIH grant CA111982. No other potential conflict of interest relevant to this article was reported.

ACKNOWLEDGMENTS

We thank Anita Ton, Juanita Weaver, Phillip Eclarinal, Alicia Forest, G. Craig Hill, George Afari, Bradford J. Wood, and Maria J. Merino for their contribution. Contract No. HHSN261200800001E. The content of this publication does not necessarily reflect the views or policies of the Department of Health and Human Services, nor does mention of trade names, commercial products, or organizations imply endorsement by the U.S. government.

REFERENCES

1. Wu JN, Fish KM, Evans CP, Devere White RW, Dall'Era MA. No improvement noted in overall or cause-specific survival for men presenting with metastatic prostate cancer over a 20-year period. *Cancer.* 2014;120:818–823.
2. Armstrong AJ, Halabi S. Making progress on progression in metastatic prostate cancer. *J Clin Oncol.* 2015;33:1322–1324.
3. Morris MJ, Molina A, Small EJ, et al. Radiographic progression-free survival as a response biomarker in metastatic castration-resistant prostate cancer: COU-AA-302 results. *J Clin Oncol.* 2015;33:1356–1363.
4. Schirrmeister H, Guhlmann A, Elsner K, et al. Sensitivity in detecting osseous lesions depends on anatomic localization: planar bone scintigraphy versus ^{18}F PET. *J Nucl Med.* 1999;40:1623–1629.
5. Even-Sapir E, Metser U, Mishani E, Lievshitz G, Lerman H, Leibovitch I. The detection of bone metastases in patients with high-risk prostate cancer: ^{99m}Tc-MDP planar bone scintigraphy, single- and multi-field-of-view SPECT, ^{18}F-fluoride PET, and ^{18}F-fluoride PET/CT. *J Nucl Med.* 2006;47:287–297.
6. Iagaru A, Mittra E, Dick DW, Gambhir SS. Prospective evaluation of Tc-99m MDP scintigraphy, F-18 NaF PET/CT, and F-18 FDG PET/CT for detection of skeletal metastases. *Mol Imaging Biol.* 2012;14:252–259.
7. Bostwick DG, Pacelli A, Blute M, Roche P, Murphy GP. Prostate specific membrane antigen expression in prostatic intraepithelial neoplasia and adenocarcinoma: a study of 184 cases. *Cancer.* 1998;82:2256–2261.
8. Chang SS, Reuter VE, Heston WD, Gaudin PB. Comparison of anti-prostate-specific membrane antigen antibodies and other immunomarkers in metastatic prostate carcinoma. *Urology.* 2001;57:1179–1183.
9. Afshar-Oromieh A, Holland-Letz T, Giesel FL, et al. Diagnostic performance of ^{68}Ga-PSMA-11 (HBED-CC) PET/CT in patients with recurrent prostate cancer: evaluation in 1007 patients. *Eur J Nucl Med Mol Imaging.* 2017;44:1258–1268.
10. Evans MJ, Smith-Jones PM, Wongvipat J, et al. Noninvasive measurement of androgen receptor signaling with a positron-emitting radiopharmaceutical that targets prostate-specific membrane antigen. *Proc Natl Acad Sci USA.* 2011;108:9578–9582.
11. Eiber M, Maurer T, Souvatzoglou M, et al. Evaluation of hybrid ^{68}Ga-PSMA ligand PET/CT in 248 patients with biochemical recurrence after radical prostatectomy. *J Nucl Med.* 2015;56:668–674.
12. Rowe SP, Macura KJ, Ciarallo A, et al. Comparison of prostate-specific membrane antigen-based ^{18}F-DCFBC PET/CT to conventional imaging modalities for detection of hormone-naive and castration-resistant metastatic prostate Cancer. *J Nucl Med.* 2016;57:46–53.
13. Pyka T, Okamoto S, Dahlbender M, et al. Comparison of bone scintigraphy and ^{68}Ga-PSMA PET for skeletal staging in prostate cancer. *Eur J Nucl Med Mol Imaging.* 2016;43:2114–2121.

14. Rowe SP, Macura KJ, Mena E, et al. PSMA-based [^{18}F]DCFPyL PET/CT is superior to conventional imaging for lesion detection in patients with metastatic prostate cancer. *Mol Imaging Biol.* 2016;18:411–419.
15. Rowe SP, Mana-Ay M, Javadi MS, et al. PSMA-based detection of prostate cancer bone lesions with ^{18}F-DCFPyL PET/CT: a sensitive alternative to ^{99m}Tc-MDP bone scan and Na^{18}F PET/CT? *Clin Genitourin Cancer.* 2016;14:e115–e118.
16. Uprimny C, Kroiss A, Nilica B, et al. ^{68}Ga-PSMA ligand PET versus ^{18}F-NaF PET: evaluation of response to ^{223}Ra therapy in a prostate cancer patient. *Eur J Nucl Med Mol Imaging.* 2015;42:362–363.
17. Cho SY, Gage KL, Mease RC, et al. Biodistribution, tumor detection, and radiation dosimetry of ^{18}F-DCFBC, a low-molecular-weight inhibitor of prostate-specific membrane antigen, in patients with metastatic prostate cancer. *J Nucl Med.* 2012;53:1883–1891.
18. Mease RC, Dusich CL, Foss CA, et al. N-[N-[(S)-1,3-Dicarboxypropyl]carbamoyl]-4-[^{18}F]fluorobenzyl-L-cysteine, [^{18}F]DCFBC: a new imaging probe for prostate cancer. *Clin Cancer Res.* 2008;14:3036–3043.
19. Surti S, Kuhn A, Werner ME, Perkins AE, Kolthammer J, Karp JS. Performance of Philips Gemini TF PET/CT scanner with special consideration for its time-of-flight imaging capabilities. *J Nucl Med.* 2007;48:471–480.
20. Shih JH, Fay MP. Pearson's chi-square test and rank correlation inferences for clustered data. *Biometrics.* 2017;73:822–834.
21. Rosner B, Glynn RJ, Lee ML. Extension of the rank sum test for clustered data: two-group comparisons with group membership defined at the subunit level. *Biometrics.* 2006;62:1251–1259.
22. Scher HI, Solo K, Valant J, Todd MB, Mehra M. Prevalence of prostate cancer clinical states and mortality in the United States: estimates using a dynamic progression model. *PLoS One.* 2015;10:e0139440.
23. Westin P, Stattin P, Damber JE, Bergh A. Castration therapy rapidly induces apoptosis in a minority and decreases cell proliferation in a majority of human prostatic tumors. *Am J Pathol.* 1995;146:1368–1375.
24. van Weerden WM, van Kreuningen A, Elissen NM, et al. Castration-induced changes in morphology, androgen levels, and proliferative activity of human prostate cancer tissue grown in athymic nude mice. *Prostate.* 1993;23:149–164.
25. Ibrahim T, Flamini E, Mercatali L, Sacanna E, Serra P, Amadori D. Pathogenesis of osteoblastic bone metastases from prostate cancer. *Cancer.* 2010;116:1406–1418.
26. Morrissey C, Vessella RL. The role of tumor microenvironment in prostate cancer bone metastasis. *J Cell Biochem.* 2007;101:873–886.
27. Meller B, Bremmer F, Sahlmann CO, et al. Alterations in androgen deprivation enhanced prostate-specific membrane antigen (PSMA) expression in prostate cancer cells as a target for diagnostics and therapy. *EJNMMI Res.* 2015;5:66.
28. Szabo Z, Mena E, Rowe SP, et al. Initial evaluation of [^{18}F]DCFPyL for prostate-specific membrane antigen (PSMA)-targeted PET imaging of prostate cancer. *Mol Imaging Biol.* 2015;17:565–574.
29. Eiber M, Fendler WP, Rowe SP, et al. Prostate-specific membrane antigen ligands for imaging and therapy. *J Nucl Med.* 2017;58:67S–76S.
30. Roudier MP, True LD, Higano CS, et al. Phenotypic heterogeneity of end-stage prostate carcinoma metastatic to bone. *Hum Pathol.* 2003;34:646–653.